# Viability of the Wankel Rotary Engine Combusting Hydrogen Fuel as an Alternative to Other Eco-Friendly Motorcycle Powerplants

Kyle Turner

January 2022

MSc Research Report
MSc Motorcycle Engineering

**Abstract**

This report attempts to analyse the viability of the Wankel rotary engine for use in motorcycles by comparing its efficiency, storage capacity of the system and mass of the power train to other eco-friendly alternatives to conventional gasoline powered reciprocating engines. Through the use of a computational flow dynamics simulation in ANSYS FLUENT a method to obtain the internal pressures of the rotary engine and NOx production has been devised to allow for the obtaining of the mean effective pressure and the emissions of the rotary engine. Through acquiring this information the Wankel rotary engine can be compared to other eco-friendly alternatives such as electric and fuel cell power trains for use in motorcycles. The power-train of a motorcycle with a Wankel Rotary Engine has been compared with that of fuel cell and electric alternatives on the basis of mass, volume, power and range.

# Contents


**1 Introduction** **4**
1.1 Introduction . . . 4
1.2 Industry Relevance . . . 4

**2 Literature Review** **5**
2.1 Overview . . . 5
2.2 The Wankel Engine: Initial Issues and Development . . . 5
2.3 Hydrogen Combustion Characteristics . . . 6
2.3.1 Laminar Flame Speed . . . 6
2.3.2 Minimum Ignition Energy . . . 6
2.3.3 Quenching Distance . . . 6
2.3.4 Flammability Limits . . . 6
2.3.5 Auto Ignition Temperature . . . 6
2.3.6 Diffusivity . . . 7
2.4 Engine Analysis . . . 7
2.5 CFD Theory . . . 8
2.6 Overview . . . 8
2.7 Continuity and Momentum Equations . . . 8
2.8 Compressible Flows . . . 8
2.9 Turbulence . . . 8
2.9.1 Standard $k - \epsilon$ . . . 9
2.9.2 RNG $k - \epsilon$ . . . 9
2.9.3 Realizable $k - \epsilon$ . . . 10
2.10 Combustion Models . . . 10
2.10.1 Overview . . . 10
2.10.2 Non-premixed Combustion Model . . . 10
2.10.3 Premixed Combustion Model . . . 11
2.10.4 Partially Premixed Combustion . . . 12
2.11 Composition PDF Transport . . . 13
2.12 Engine Ignition . . . 14
2.13 NOx Formation . . . 15

**3 Methodology** **16**
3.1 CFD . . . 16
3.1.1 Overview . . . 16
3.1.2 Geometry . . . 16
3.1.3 Meshing . . . 16
3.2 Rotor Movement . . . 17
3.2.1 Simulation Setup . . . 17
3.3 Data Analysis . . . 18

**4 Results** **18**

**5 Discussion** **18**
5.1 Viability of the Engine . . . 19
5.1.1 Emissions . . . 19
5.1.2 Power . . . 19
5.1.3 Range . . . 19

**6 Conclusions** **19**

**7 Further Work** **20**

# 1 Introduction

## 1.1 Introduction

With the introduction of zero tailpipe emission laws there is now an imminent requirement for green alternatives to gasoline and diesel fueled internal combustion engines, such as hydrogen fuel cells, electric, hydrogen internal combustion engines or combining the previous two, in series hybrid. Given the large body of data on fuel cell and electric vehicles this report will focus on the Wankel rotary engine and analyse it as a contender against electric and hydrogen fuel cell powertrains for motorcycle use.

Since its invention in 1957 the Wankel rotary engine has been studied, however interest in the engine within industry decreased due to high emissions caused by incomplete combustion and the necessity to have lubricant within the combustion chamber. The first simulations were developed in the 1980s however, relative to 2-stroke and 4-stroke reciprocating engines the volume of work has remained small, with few companies in industry continuing to produce Wankel engines. This project intends to expand the understanding of the Wankel engine and identify if it is suitable for usage in motorcycles as we move to a greener future. Hydrogen has been evaluated as fuel in Wankel rotary engines since the 1970s (Cichanowicz and Sawyer, 1976), and technology has developed heavily in materials and machining capabilities, with Mazda finding low NOx emissions in their hydrogen fueled RENESIS engine in 2006(Wakayama et al., 2006). Despite these improvements rotary engines continue to only have niche uses within industry, such as UAVs, with no current large-scale commercial Wankel engine motorcycles or cars in production. There is however, an interest beginning to develop for using Wankel rotary engines as range extenders in series hybrid vehicles operating at a single RPM to minimise NOx production(Salanki and Wallace, 1996).

In this report a simulation of a hydrogen fueled Wankel rotary engine will be created in order to investigate the performance and emissions of the engine and help determine if it is a viable contender to other green alternatives. Given the theoretical low cost of mass manufacture of Wankel rotaries it may also prove inexpensive to produce motorcycles powered by them as compared to battery and fuel cells. The Advanced Innovative Engineering 80S will be used for the simulation. Whilst originally experimental data collection was planned in order to directly validate data collected from the simulation, due to time constraints this was not achieved. Finally the data obtained from the simulation, engine core mass and information on fuel storage methods will be collected and used to evaluate the Wankel Rotary Engine as a negligible emission alternative to electric and hybrid powertrains.

## 1.2 Industry Relevance

The Wankel RE has long been of interest to the motorcycle industry, with some manufacturers, such and Hercules, Norton and Suzuki producing commercial models to little success. With the introduction of zero-emission laws, such as the UK governments, it is more important than ever for clean alternatives to gasoline powered internal combustion engines to be developed. The Wankel RE has been experimented with using hydrogen as a fuel since the 1990s by Mazda for their rotary engine cars. Hydrogen Wankel REs have been found to have very low emissions (Wakayama et al., 2006), are particularly well suited to hydrogen combustion as it minimises the difficulties a reciprocating engine suffers (Salanki and Wallace) and could be low cost to manufacture, making them a viable alternative to electric motorcycles. The Wankel RE is particularly well suited to motorcycle usage give its light weight, higher revs and vibration-free engine. However, given its previously terrible emissions the design has seen little interest in the industry since Norton produced theirs in the 80s, with them mostly being used for UAVs. With the development of materials in the 21st century it is now possible to resolve many of the rotary engine's issues and create motorcycles, such as Crighton motorcycles CR700W (www.crightonmotorcycles.com, n.d.), which produce power outclassing competitors. As Wankel rotary engine can theoretically be created at low cost, produce negligible emissions using hydrogen as a fuel and if they can maintain range comparable to other green motorcycles they would serve as a strong competitor for modern motorcycles.

The ethics of producing eco-friendly motorcycles must also be considered, as we switch to green alternatives the materials required to produce components such as batteries come not just at high monetary cost but also human and environmental cost, given it is well known that the mining of cobalt, a material used in batteries, often utilises child labour and destroys the prospecting of which causes mass ecological destruction (McKie, 2021). Additionally once these rare materials have been siphoned up by the developed world it is both unethical and impossible to demand that lesser developed countries stop using fossil fuels without providing affordable alternatives. It is possible that the Wankel engine could be this alternative. The limiting factors in running motorcycles on hydrogen fuel are the lack of current hydrogen fuel infrastructure, the difficulties in storing significant amounts of hydrogen and the safety implications. However, fuel cell vehicles have long been a proven concept which use hydrogen as a fuel, the safety of such vehicles has long been tested and countries have shown that they are willing to create the infrastructure for hydrogen pumps. A significant benefit of hydrogen compared to electric vehicles is that hydrogen vehicles do not have a refill time too different from gasoline unlike the minutes to hours that electric vehicles have. Additionally, whilst the storage capacity of hydrogen is limited there is little need for a replacement as, unlike batteries, the capacity of the tanks will not decrease with time.

# 2 Literature Review

Analysis of hydrogen combustion is a subject area that has been intensely studied, with many papers discussing the characteristics of the combustion. The work by Hanson and Salimian (1984) has surveyed the rate constants in N/H/O reactions, allowing others to reference these constants for use in other areas, such as CFD.

The equations describing the motion of the a Wankel rotary engine are well documented (Yamamoto, k, 1981) which allows in depth analysis of volume changes of the engine throughout motion.

Sierens et al. (1983) developed a model to simulate a Wankel rotary engine, validating it against experimental data obtained by G. Wolters, wherein the data was collected using a static rotor with a rotating housing. The model developed is based off a reciprocating engine model and shares the same assumptions. Due to the movement of the air being due to energy exerted on it by the casing, not the rotor, it is possible turbulence effects of the rotor have not been accurately displayed which will negatively affect the quality of the information.

Farzadi, A (2015) has created a cold flow analysis in ANSYS Fluent v.15 however due to using a 2D model for their results they have found pressure values higher than the realistic values. Whilst combustion was not included they do recommend using a symmetric model due to it having better physical distribution. They also assert that inlet flows must also be modelled in order to create an accurate picture as these flows affect the mixture long after the port has closed. The author goes into a lot of detail on the CFD modelling in Fluent V.15 which is of great value to this project.

Salvi, B.L et al. (2016) performed experimental tests on a reciprocating engine using hydrogen as a fuel. They found that NOx emissions significantly increased with compression ratio, additionally through use of an EGR of 20% it was possible to reduce NOx generation by 50% with marginal effect on power and brake thermal efficiency. Despite this being a reciprocating engine this information is relevant to the Wankel rotary as these effects are due to Hydrogen's combustion characteristics.

Salanki, P.A. et al. (1996) evaluated the hydrogen fueled wankel engine for hybrid usage and found it to be promising, however they note that there is a possibility for hydrogen peroxide to form in leaner mixtures. They further suggest that a hydrogen fuel necessitate less lubrication as there are fewer carbon build-ups on the surface of the chamber.

Building on to the work of Salanki, P.A. et al. (1996), Di Ilio, G. et al. (2020) have replaced a reciprocating engine with a rotary engine in a hydrogen series-hybrid car in order to evaluate the rotary engine as an alternative power plant. To do this they evaluated 6 vehicles of similar mass, a baseline electric car, one fitted with a gasoline fueled reciprocating engine, one with a gasoline fueled rotary engine and three hydrogen fueled rotary engines with differing fuel tank sizes. From this study they found the largest tanked hydrogen fueled rotary engine vehicle out performed the gasoline fueled electric vehicle in range, however it is worth noting that the energy density and mass of the carried hydrogen fuel was significantly less than that of the gasoline and as such as hydrogen tank designs improve so will range the these vehicles.

## 2.1 Overview

## 2.2 The Wankel Engine: Initial Issues and Development

The Wankel rotary engine was patented in 1929 by Felix Wankel, with the first working prototype being completed in 1957. It's high power to weight ratio, the lack of vibrations when running and few moving parts made the engine attractive for automotive and aviation purposes. The Wankel RE uses the Otto cycle and is characterised by a triangular rotor inside an oval-like epitrochoidal housing. The output shaft is toothed to rotate three times for every rotation of the rotor, resulting in a total crank angle of 1080 degrees, with each face of the rotor is working simultaneously. As each rotor face undergoes a different stage of the Otto cycle at the same time this means there is one power pulse per crankshaft rotation, similar to a two-stroke reciprocating engine.

Despite the possible benefits of the engine it has long been plagued with issues. Combustion issues due to its long, narrow and moving combustion chamber, issues with apex seal leakage, rotor sealing issues and high temperature gradients across the engine. The combustion chambers long and narrow design makes it unsuited to gasoline combustion due to gasoline's slow combustion speed and large quenching distance (Cracknel et al.,2002), this is further compounded by the direction of combustion being the same as the direction of chamber movement resulting in unburnt hydrocarbons, originating in the trailing side of the combustion chamber(Muroki and Fujimoto, 1987), being sent to the exhaust. Due to combustion occurring in only one section of the engine a heat differential is created across the engine. The intake stroke and compression stroke occur in a cool section and the combustion and exhaust strokes occur in a hot section. This creates difficulties in sealing as the apex seals must adapt to varying amounts of expansion. Additionally, the apex seals can begin to lift off the surface of the chamber allowing gases to leak between chambers, reducing the overall efficiency of the engine (Li, et al., 1991). These factors mean the Wankel engine was found to have high fuel consumption, high emissions and a lower thermal efficiency as compared to conventional four-stroke reciprocating engine and as such have not been favoured by the automotive and motorcycle industries, despite some early endeavours.

However, the issues of the engine has not stopped the development of the Wankel rotary engine, Mazda produced an RE car up until 2012 and the engine has found use in unmanned aerial vehicles (UAV) where the high power to weight ratio and few moving parts are especially important. With few manufacturers holding an interest in the Wankel

rotary engine its development has been slow however significant improvements have been made due to design changes and developments in materials. The Mazda Renesis engine (Ohkubo et al., 2004) uses a number of technologies to improve the combustion process within the engine. The peripheral exhaust and intake ports have been replaced with side exhaust ports, this stops early opening of the exhaust port, allowing for a longer expansion stroke and also stops intake/exhaust port overlap, meaning no exhaust gases are exchanged with another chamber undergoing the intake stroke. Advanced Innovative Engineering uses the Self-Pressurising-Air Rotor Cooling System in their rotary engine, the SPARCS utilises the self-pressurising blow by gases from the combustion process as a cooling medium. The gases escape into the interior of the engines core and are recirculated in a closed loop by a fan driven by the main shaft, the air-gas mixture is circulated multiple times before reentering the combustion chamber and being burnt away. This reduces lubricant consumption, reducing emissions and reduces the temperature gradient across the engine. These developments suggest that, despite few manufacturers working with rotary engines, the engines primary issues are beginning to be reduced and there's likely still potential to improve the engines further.

## 2.3 Hydrogen Combustion Characteristics

Hydrogen combustion differs from gasoline in many ways and there upsides and downsides to these differences, this section will discuss these characteristics in detail. Table 1 shows some of the characteristics of hydrogen and gasoline fuels. In general combustion of hydrogen can be highly energy intensive, resulting temperatures that lead to the creation of nitrous oxides, a significant greenhouse gas.

| | Hydrogen | Gasoline |
|---|---|---|
| Burning velocity at stoichiometric conditions | 3.24 m/s | 0.47 m/s |
| Quenching Gap | 0.6mm | 2mm |
| Lean flammability limit at atmospheric conditions | $\lambda = 7.4$ | $\lambda = 1.8$ |

Table 1: Combustion characteristics of hydrogen, adopted from Cracknell et al. (2002)

### 2.3.1 Laminar Flame Speed

The higher combustion speed of hydrogen means it has a greater heat release rate, this results in a higher temperature and accordingly, cooling losses. The higher laminar flame speed also affects the combustion stability, resulting in a "knocking" effect in conventional piston driven engines. The burn velocity of hydrogen fuel is reduced in a Wankel rotary engine as the combustion chamber moves in the same direction as the flame front, smoothing out the energy release.

### 2.3.2 Minimum Ignition Energy

The minimum ignition energy of a fuel is the energy required to begin combustion. The minimum combustion energy of hydrogen-air mixture is 0.02MJ which is significantly lower than the 0.24MJ of a gasoline-air mixture, this means that a hydrogen fuel is much more likely to pre-ignite on hot spots in the combustion chamber. The Wankel rotary engine's design is inherently resistant to pre-ignition events as the intake/compression areas of the engine are separate to the combustion/exhaust areas, meaning the air-fuel mixture only encounters hot-spots when ignition is desired.

### 2.3.3 Quenching Distance

The distance between two surfaces which a flame front can no longer propagate is the quenching distance, the quenching distance of hydrogen is 0.6mm, this means more of the air-fuel mixture is available for combustion. The flame front propagates closer to the wall of the chamber which increases cooling losses, this also means the air-fuel mixture is in closer proximity to areas of high temperature such as spark plugs, exhaust valves which can cause pre-ignition. As previously discussed this is of lesser issue in a Wankel rotary engine due to it being resistant to pre-ignition events.

### 2.3.4 Flammability Limits

Due to hydrogen's wide flammability limits it can operated in highly rich or lean mixtures, especially as compared to gasoline. This is useful as when burned stoichiometrically the high temperatures generated produce large amounts of nitrous oxides (NOx), thus leaner mixtures will provide better emissions and fuel economy due to a more complete combustion.

### 2.3.5 Auto Ignition Temperature

The auto ignition temperature (AIT) of an air-fuel mixture is the temperature at which it will self-ignite, the compression ratio of a fuel is intrinsically linked to the AIT with a higher AIT correlating to a higher compression ratio. Hydrogen's AIT is higher than that of gasoline and thus more power can be generated from the engine, this power is

however limited by a particular engine's design, as Wankel rotary engines suffer from low compression ratios due to its geometry.

#### 2.3.6 Diffusivity

Hydrogen is significantly more diffusive than gasoline which provides benefits as a fuel and in safety. The high diffusivity lends to a more perfect fuel-air mixture, this coupled with the longer intake stroke of the Wankel rotary engine lends to a better fuel mixture. Should any leakage occur from the storage tank or the engine the diffusivity of the hydrogen would lead to rapidly reaching its flammability limit.

### 2.4 Engine Analysis

Engine performance is defined by Heywood, J.B. (2018) as the maximum power (or maximum torque) available at each speed within the useful engine operating speed and the range of speed and power over which engine operation is satisfactory. However, there are a number of parameters which be measured to discuss the performance of a particular engine. Engine torque is calculated using a dynamometer, wherein the engine's output shaft is coupled to the dynamometer, allowing the torque to be calculated. Power delivered by the engine is the product of torque and angular speed:

$$P = 2\pi NT \tag{1}$$

Where $N$ is the rotational speed of the crankshaft and $T$ is the torque. This the "brake power", the usable power which is delivered by the engine.

Cylinder pressure and volume data can be plotted on a P-V diagram, by integrating around the curve we obtain the indicated work per cycle. This differs from brake power in the power required to overcome engine friction and driving engine accessories. Two values of indicated work per cycle can be collected, "gross", the work delivered to the piston over compression and expansion strokes only and "net", the work delivered over the whole cycle. There is much difficulty is collecting this data for a rotary engine as the combustion chamber moves as it changes in volume, Vorraro, G. et al. (2018) describes an approach wherein multiple transducers are placed around the periphery of the trochoid and a program is used to combine the data from each transducer per chamber, allowing for the collection of pressure data. The volume is calculated for the movement of the chamber and the data combined and plotted. The mechanical efficiency of an engine is the ratio of brake power delivered by an engine to the indicated power.

The mean effective pressure (MEP) is a useful relative measure of an engine's performance, it does not calculate torque, which is relative to engine size. MEP is calculated by the work per cycle by cylinder volume displaced per cycle:

$$mep = \frac{Pn_r}{V_d N} \tag{2}$$

Where $n_r$ is the the number of crankshaft revolution per power stroke and $V_d$ is the volume displaced or swept per cycle. By definition MEP is given by:

$$mep = \frac{W}{V_d} \tag{3}$$

Where $W$ is the work done per cycle. Using equation 3 we can calculated the indicated mean effective pressure from calculating the work done per cycle. Specific fuel consumption is the mass flow per unit time per power produced, with lower values being preferred:

$$sfc = \frac{m_f}{P} \tag{4}$$

Where $m_f$ is the mass flow rate,

Thermal efficiency relates the power, fuel flow rate and the heating value of a fuel to create a more valuable measure of efficiency:

$$\eta_f = \frac{P}{m_f Q_{HV}} \tag{5}$$

Where $Q_{HV}$ is the heating value of a fuel. Heywood, J.B. (2018) refers to this as the fuel conversion efficiency as it describes the quantity more precisely. Due to the design of the combustion chamber a Wankel engine generally has a lower fuel conversion efficiency than reciprocating engines of similar power.

The specific weight and specific volume must also be considered when investigating performing engine comparisons and are simply given by $\frac{engineweight}{ratedpower}$ and $\frac{enginevolume}{ratedpower}$ respectively. The Wankel rotary engine is known for its high power to weight ratio, and as such when discussing Wankel rotary engines and hydrogen as a green alternative the fuel storage and engine must be considered together and compared to fuel-cell and battery-motor setups.

Finally the emissions of the engine must be considered, as a particular engine must pass current regulations in order to be allowed in production vehicles. With hydrogen as a fuel the only emission of interest should be NOx. However, the engine also burns lubricant whilst it runs, generating small amounts of CO2.

## 2.5 CFD Theory

## 2.6 Overview

Computational Fluid Dynamics allows a researcher to perform what would normally be expensive tests for a relatively low cost but increased time. With increasing capabilities of computer hardware performing CFD testing has become increasingly accessible and low in cost. ANSYS FLUENT is a commercial software that is part of the ANSYS Simulation Software package, providing many tools to simulate the internal combustion engine. This section is dedicated to the theory behind the models used to create the engine simulation in this report and information has been obtained from the ANSYS FLUENT Theory Guide.

## 2.7 Continuity and Momentum Equations

The equation for conservation of momentum can be written as follows:

$$\frac{\partial \rho}{\partial t} + \nabla \cdot (\rho \overrightarrow{v}) = S_m \tag{6}$$

Conservation of momentum in an inertial reference frame is described by:

$$\frac{\partial}{\partial t} + \nabla \cdot (\rho \overrightarrow{v} \overrightarrow{v}) = -\nabla p + \nabla \cdot (\overline{\overline{\tau}}) + \rho \overrightarrow{g} + \overrightarrow{F} \tag{7}$$

Where $p$, $\overline{\overline{\tau}}$, $\rho \overrightarrow{g}$, $\overrightarrow{F}$, are the static pressure, the stress tensor the gravitational body force and external body forces respectively. $\overline{\overline{\tau}}$ is given by the following equation:

$$\overline{\overline{\tau}} = \mu \left[ (\nabla \overrightarrow{v} + \nabla \overrightarrow{v}^T) - \frac{2}{3} \nabla \cdot \overrightarrow{v} I \right] \tag{8}$$

Where $\mu$ is the molecular viscosity, $I$ is the unit tensor.

## 2.8 Compressible Flows

Compressibility effects are encountered when gas flow is at high velocity or there are large pressure variations. When flow velocity or pressure change is large the variation of gas pressure with density has significant effects on temperature, flow velocity and pressure. Compressible flows are characterised by the Mach number described by the equation:

$$M \equiv \mu / c \tag{9}$$

Where c is the speed of sound the gas:

$$c = \sqrt{\gamma R T} \tag{10}$$

Where $\gamma$ is the ratio of the specific heats of the gas.

Compressible flows are characterised by the total pressure and total temperature of the flow, $P_0$ and $T_0$, respectively. These quantities are related to static pressure and temperature via the following:

$$\frac{p_0}{p} = exp \left( \frac{\int_T^{T_0} \frac{C_p}{T} dT}{R} \right) \tag{11}$$

With a constant value for $C_p$ the above equation becomes:

$$\frac{p_0}{p} = \left( 1 + \frac{\gamma - 1}{2} M^2 \right)^{\gamma/(\gamma-1)} \tag{12}$$

$$\frac{T_0}{T} = 1 + \frac{\gamma - 1}{2} M^2 \tag{13}$$

## 2.9 Turbulence

ANSYS FLUENT has multiple options for turbulence modelling, for the $k - \epsilon$ model is has three variations; Standard, RNG and Realizable. Whilst ANSYS FLUENT does have other turbulence models, the $k - \epsilon$ model is very popular for engine simulations so this section will only discuss these models.

### 2.9.1 Standard $k-\epsilon$

The standard $k$-$\epsilon$ model is a semi-empirical mode based on transport equations for turbulent kinetic energy, k, and turbulent dissipation rate, $\epsilon$. $k$ and $\epsilon$ are obtained from the following transport equations:

$$\frac{\partial}{\partial t}(\rho k) + \frac{\partial}{\partial x_i}(\rho k u_i) = \frac{\partial}{\partial x_j}\left[\left(\mu + \frac{\mu_t}{\sigma_k}\right)\frac{\partial k}{\partial x_j}\right] + G_k + G_b - \rho\epsilon - Y_M + S_k \tag{14}$$

$$\frac{\partial}{\partial t}(\rho \epsilon) + \frac{\partial}{\partial x_i}(\rho \epsilon u_i) = \frac{\partial}{\partial x_j}\left[\left(\mu \frac{\mu_t}{\sigma_\epsilon}\right)\frac{\partial \epsilon}{\partial x_j}\right] + C_{1\epsilon}\frac{\epsilon}{k}(G_k + C_{3\epsilon}G_b) - C_{2\epsilon}\rho\frac{\epsilon^2}{k} + S_\epsilon \tag{15}$$

The values of $G_k$, $G_b$, $Y_M$ represents the generation of turbulence kinetic energy due to the mean velocity gradients, the generation of kinetic energy due to buoyancy, the contribution of fluctuating dilation in compressible turbulence to the overall dissipation rate respectively. $C_{1\epsilon}$,$C_{2\epsilon}$ and $C_{3\epsilon}$ are constants. $\sigma_k$ and $\sigma_\epsilon$ are the turbulent Prandtl numbers for $k$ and $\epsilon$. $S_k$ and $S_\epsilon$ are user defined source terms. $\mu_t$, the turbulent viscosity is computed by combining $k$ and $\epsilon$:

$$\mu_t = \rho C_\mu \frac{k^2}{\epsilon} \tag{16}$$

Where $C_\mu$ is a constant. The values of $C_{1\epsilon}$, $C_{2\epsilon}$, $C_\mu$, $\sigma_k$ and $\sigma_\epsilon$ have been determined from experiments and are as follows: $C_{1\epsilon} = 1.44$, $C_{2\epsilon} = 1.92$, $C_\mu = 0.09$, $\sigma_k = 1.0$ and $\sigma_\epsilon = 1.3$.

### 2.9.2 RNG $k-\epsilon$

The RNG $k-\epsilon$ model has been derived from a statistical technique called renormalization group theory, it is similar to the standard $k-\epsilon$ model with some modifications. The transport equations for the RNG $k-\epsilon$ model are as follows:

$$\frac{\partial}{\partial t}(\rho k) + \frac{\partial}{\partial x_i}(\rho k u_i) = \frac{\partial}{\partial x_j}\left(\alpha_\epsilon \mu_{eff}\frac{\partial k}{\partial x_j}\right) + G_k + G_b - \rho\epsilon - Y_M + S_k \tag{17}$$

$$\frac{\partial}{\partial t}(\rho \epsilon) + \frac{\partial}{\partial x_i}(\rho \epsilon u_i) = \frac{\partial}{\partial x_j}\left(\alpha_\epsilon \mu_{eff}\frac{\partial \epsilon}{\partial x_j}\right) + C_{1\epsilon}\frac{\epsilon}{k}(G_k + C_{3\epsilon}G_b) - C_{2\epsilon}\rho\frac{\epsilon^2}{k} + -R_\epsilon - S_\epsilon \tag{18}$$

The values $\alpha_k$ and $\alpha_\epsilon$ are the inverse effective Prandtl numbers for $k$ and $\epsilon$. Due to the scale elimination procedure in the RNG $k-\epsilon$ model a differential equation is generated for turbulent viscosity:

$$d\left(\frac{\rho^2 k}{\sqrt{\epsilon\mu}}\right) = 1.72\frac{\hat{\upsilon}}{\sqrt{\hat{\upsilon}^3 - 1 + C_\upsilon}}d\hat{\upsilon} \tag{19}$$

$$\hat{\upsilon} = \frac{\mu_{eff}}{\mu}, C_\upsilon \approx 100$$

The above equation is integrated to obtain an accurate description of how the effective turbulent transport varies with the effective Reynolds number. At the high Reynolds-number limit the equation becomes:

$$\mu_t = \rho C_\mu \frac{k^2}{\epsilon} \tag{20}$$

With $C_\mu = 0.0845$, derived using RNG theory. The RNG model allows for the effects of swirl on turbulent viscosity through the modification of the term $\mu_t$:

$$\mu_t = \mu_{t0} f\left(\alpha_s, \Omega, \frac{k}{\epsilon}\right) \tag{21}$$

Where $\mu_{t0}$ is the value of turbulent viscosity without the swirl modification. $\Omega$ is an evaluated swirl factor calculated within ANSYS Fluent and $\alpha_s$ is a swirl constant depending on whether the flow is swirl-dominated or not. The inverse Prandtl numbers, $\alpha_k$ and $alpha_\epsilon$ are computed from the following formula:

$$\left|\frac{\alpha - 1.3929}{\alpha_0 - 1.3929}\right|^{0.6321}\left|\frac{\alpha + 2.3929}{\alpha_0 + 2.3929}\right|^{0.3679} = \frac{\mu_{mol}}{\mu_{eff}} \tag{22}$$

The primary difference between the standard and RNG $k-\epsilon$ model is in the term $R_\epsilon$, this term is given by the following calculation:

$$R_\epsilon = \frac{C_\mu \rho \eta^3 (1 - \eta/\eta_0)\epsilon^2}{1 + \beta\eta^3}\frac{\epsilon^2}{k} \tag{23}$$

where

$$\eta = Sk/\epsilon, \eta_0 = 4.38, \beta = 0.012$$

The model constants $C_{1\epsilon}$ and $C_{2\epsilon}$ are derived analytically have values of 1.42 and 1.68 respectively. The RNG model is more responsive to rapid changes in strain and streamline curvature than the standard model which results in superior performance in some simulations.

### 2.9.3 Realizable $k-\epsilon$

The realizable model differs from the the standard model in that it has a new formula for the turbulent velocity and uses a different equation for the transport rate, $\epsilon$, derived from an exact equation for the transport of the mean-square vorticity fluctuation. The transport equations of the realizable model are given by:

$$\frac{\partial}{\partial t}(\rho k) + \frac{\partial}{\partial x_j}(\rho k u_j) = \frac{\partial}{\partial x_j}\left[\left(\mu\frac{\mu_t}{\sigma_k}\right)\frac{\partial k}{\partial x_j}\right] + G_k + G_b - \rho\epsilon - Y_M + S_k \tag{24}$$

and

$$\frac{\partial}{\partial t}(\rho \epsilon) + \frac{\partial}{\partial x_j}(\rho \epsilon u_j) = \frac{\partial}{\partial x_j}\left[\left(\mu + \frac{\mu_t}{\sigma_\epsilon}\right)\frac{\partial \epsilon}{\partial x_j}\right] + \rho C_1 S_\epsilon - \rho C_2 \frac{\epsilon^2}{k+\sqrt{\eta\epsilon}} + C1\epsilon\frac{\epsilon}{k}C_{3\epsilon}G_b + S_\epsilon \tag{25}$$

where

$$C_1 = max\left[0.43, \frac{\eta}{\eta+5}\right], \eta = S\frac{k}{\epsilon}, S = \sqrt{2SijSij}$$

The turbulent viscosity is calculated the same as in other models:

$$\mu_t = \rho C_\mu \frac{k^2}{\epsilon}$$

With $C_\mu$ not being a constant. $C_\mu$ is calculated from:

$$C_\mu = \frac{1}{A_0 + A_S\frac{kU^*}{\epsilon}} \tag{26}$$

where

$$U^* \equiv \sqrt{SijS_{ij} + \tilde{\Omega}_{ij}\tilde{\Omega}_{ij}}$$

$$\tilde{\Omega}_{ij} = \Omega_{ij} - 2\epsilon_{ijk}\omega_k$$

$$\Omega_{ij} = \overline{\Omega_{ij}} - \epsilon_{ijk}\omega_k$$

Where $\overline{\Omega_{ij}}$ is the mean rate of rotation tensor in a reference with angular velocity of $\omega_k$

$$A_0 = 4.04, A_s = \sqrt{6}cos\theta$$

$$\theta = \frac{1}{3}cos^{-1}(\sqrt{6}W), W = \frac{S_{ij}S_{jk}S_{ki}}{\tilde{S}^2}, \tilde{S} = \sqrt{S_{ij}S_{ij}}, S_{ij}\frac{1}{2}\left(\frac{\partial u_j}{\partial x_i} + \frac{\partial u_i}{\partial x_j}\right)$$

$$C_{1\epsilon} = 1.44, C_2 = 1.9, \sigma_k = 1.0, \sigma_\epsilon = 1.2$$

The compressible form of the ideal gas law is given by:

$$\rho = \frac{p_{op} + p}{\frac{R}{W_\omega}T} \tag{27}$$

## 2.10 Combustion Models

### 2.10.1 Overview

ANSYS FLUENT has a number of combustion models, of which this report is interested in the non-premixed combustion model, the premixed combustion model and the partially premixed combustion model. The partially premixed combustion model is a combination of the non-premixed and the premixed combustion model.

### 2.10.2 Non-premixed Combustion Model

In a non-premixed combustion the fuel and oxidiser enter the combustion chamber in separate streams. For simplicity thermochemistry is reduced to a single parameter in the non-premixed combustion model, the mixture fraction, $f$. This is the local fraction of burnt and unburned elements in all species and is a conserved quantity. This simplifies combustion to a mixing problem where, once mixed, can be modelled with the Equilibrium model, the Steady Laminar Flamelet model or the Unsteady Laminar Flamelet model, dependent upon the values of the stream. Using the values of the mixture fraction the thermochemistry calculations are preprocessed for look up in ANSYS FLUENT with the interaction of turbulence and chemistry being accounted for by a Probability Density Function. The mixture fraction, written in terms of atomic mass is given by:

$$f = \frac{Z_i - Zi, ox}{Z_{i,fuel} - Z_{i,ox}} \tag{28}$$

Where $Z_i$ is the mass fraction of element $i$ the subscript $_ox$ os the value at the oxidiser stream inlet and $_fuel$ is the value at the fuel stream inlet. If it is assumed that the species have equal diffusivities, a single equation can be used for the mixture fraction. The transport equations for the mixture fraction are given by:

$$\frac{\partial}{\partial t}(\rho \bar{f}) = \nabla \cdot \left( \frac{\mu_t}{\sigma_t} \nabla \bar{f} \right) + S_m + S_{user} \tag{29}$$

The mixture fraction, $f$ can be related to the equivalence ratio, *theta* via the following equation:

$$f = \frac{\phi}{\phi + r} \tag{30}$$

Where $r$ is the mass air-fuel ratio. For a non-adiabatic system the instantaneous species mass fraction, temperature or density is parameterised as:

$$\phi_i = \phi_i(f, H) \tag{31}$$

Where H is the instantaneous enthalpy. The probability density functon, $p(f)$ can be written as:

$$p(f)\Delta f = \lim_{T \to \infty} \frac{1}{T} \sum_i \tau_i \tag{32}$$

Where T is the time scale, $\tau_i$ is the time $f$ spend in the $\delta f$ band. The shape of the PDF, $p(f)$, is given by the double delta function or the $\beta$-function with the double delta function being most easily computed and the *beta*-function being more accurate to experimental results. The double delta function is:

$$p(f) = \begin{cases} 0.5 & f = \bar{f} - \sqrt{\bar{f}^2} \\ 0.5 & f = \bar{f} + \sqrt{\bar{f}^2} \\ 0 & elsewhere \end{cases} \tag{33}$$

The $\beta$-function is given by a function of the mean mixture fraction, $\bar{f}$, and the mixture fraction variance, $\bar{f}'^2$:

$$p(f) = \frac{F^{\alpha-1}(1-f)^{\beta-1}}{\int f^{\alpha-1}(1-f)^{\beta-1} df} \tag{34}$$

Where

$$\alpha = \bar{f} \left[ \frac{\bar{f}(1-\bar{f})}{\bar{f}'^2} - 1 \right]$$

$$\beta = (1-\bar{f}) \left[ \frac{\bar{f}(1-\bar{f})}{\bar{f}'^2} \right]$$

For a non-adiabatic model the PDF must include enthalpy. However, this complicates the equation significantly and cannot be easily computed. In order to simplify the problem the enthalpy fluctuation are assumed to be independent of the enthalpy level. Under this assumptions we find $p(f, H) = p(f)\delta(H - \bar{H})$ and mean scalars can be calculated via:

$$\bar{\phi}_i = \int_0^1 \phi_i(f, \bar{H}) p(f) df \tag{35}$$

In order to determine the value of $\bar{\phi}_i$ a transport equation for enthalpy is required, this is given by:

$$\frac{\partial}{\partial t}(\rho \bar{H}) + \nabla \cdot (\rho \overrightarrow{v} \bar{H}) = \nabla \cdot \left( \frac{k_t}{c_p} \nabla \bar{H} \right) + S_h \tag{36}$$

Where $S_h$ is the source terms for heat transfer to wall boundaries, radiation, and heat exchange with the dispersed plane.

### 2.10.3 Premixed Combustion Model

In a premixed combustion the fuel and oxidiser are mixed together, with combustion occurring as the flame travels from burnt components to unburned. The difficulty in a premixed combustion is that the flamefront occurs as a thin propagating flame that can be stretched and contorted by turbulence. Premixed combustion is only valid for turbulent subsonic flows, and cannot be used in conjunction with pollutant models. Premixed combustion additionally, cannot simulate reacting discrete phase particles as this would result in an imperfect premixed mixture. The propagation of the flame front is calculated using a transport equation for a density-weighted mean reaction progress variable, $c$.

$$\frac{\partial}{\partial t}(\rho c) + \nabla \cdot (\rho \overrightarrow{v} c) = \nabla \cdot \left( \frac{\mu_t}{Sc_t} \nabla c \right) + \rho S_c \tag{37}$$

Where $Sc_t$ and $S_c$ is the turbulent Schmidt number and the reaction progress source variable, respectively.

$$c = \frac{\sum_{i=1}^{n} y_i}{\sum_{i=1}^{n} y_{i,eq}} \tag{38}$$

Where $n$, $Y_i$, $Y_{i,eq}$ are the number of products, mass fraction of species $i$ and equilibrium mass fraction of product species $i$. With this definition $c = 0$ where the mixture is unburned and $c = 1$ where the mixture is burned.

$$\rho S_c = \rho_u U_t |\nabla c| \tag{39}$$

Where $\rho_u$ and $U_t$ are the density of unburned mixture and the turbulent flame speed respectively. Prediction of the turbulent flame speed, $U_t$, is influenced by laminar flame speed and the flame front wrinkling, stretching and thickening. The Zimont turbulent flame speed is calculated using a model for wrinkled and thickened flame fronts:

$$\begin{aligned} U_t &= A(u')^{3/4} U_l^{1/2} \alpha^{-1/4} l_t^{1/4} \\ &= A u' \left( \frac{\tau_t}{\tau_c} \right)^{1/4} \end{aligned} \tag{40}$$

Where $A$ is the model constant, $u'$ is RMS velocity, $U_l$ is the laminar flame speed, $\alpha$ is the heat transfer coeff of unburned mixture $l_t$ is the turbulent length scale, $\tau_t$ is the turbulent time scale, $\tau_c$ is the chemical time scale. $l_t$ is calculated from:

$$l_t = C_D \frac{(u')^3}{\epsilon} \tag{41}$$

Wall quenching is not included in this model however to approximate the effect on wall quenching ANSYS FLUENT has a constant multiplier for turbulent flame speed, $\alpha_\omega$ such that $U_t$ becomes:

$$U_t = \alpha_\omega A u' \left( \frac{\tau_t}{\tau_c} \right)^{1/4} \tag{42}$$

$\alpha_\omega$'s default value is 1, with values greater than 1 increasing the flame speed, and values from 1 to 0 decreasing it. In the non-adiabatic premixed combustion model the temperature is calculated by using a transport equation to account for heat gains and losses. The energy equation is given by:

$$\frac{\partial}{\partial h} + \nabla \cdot (\rho \overrightarrow{v} h) = \nabla \left( \frac{k + k_t}{c_p} \right) + S_{h,chem} + S_{h,rad} \tag{43}$$

Where $h$ is the sensible enthalpy, $S_{h,chem}$ is the heat gains from the reaction and $S_{h,rad}$ is heat loss due to radiation. Density is calculated using the ideal gas law, for the non-adiabatic system is calculated using:

$$\rho T = \rho_u T_u \tag{44}$$

Where T is calculated from the energy transport equation, $\rho_u$ is the unburned density and $T - u$.

### 2.10.4 Partially Premixed Combustion

The partially premixed combustion model is based on both the premixed and non-premixed models. The premixed reaction progress variable $c$ determines the position of the flame front. Behind the flame front the mixture is burned and either the equilibrium or laminar flame front mixture solution is used. Ahead of the flame front, the species mass fractions, density and temperature are calculated from the mixed but unburned fraction. Within the flames a linear combination of both burned and unburned mixture is used. The theory, limitations and assumptions of both the premixed and non-premixed models apply directly the the partially pre-mixed model. The density weighted scalars, such as species fractions and temperature are calculated from the PDF function of $f$ and $c$:

$$\bar{\phi}] \int_0^1 \int_0^1 \phi(f,c) p(f,c) df dc \tag{45}$$

Assuming thin flames, such that only unburned and burned mixtures exist:

$$\bar{\phi} = \bar{c} \int_0^1 \phi_b(f) p(f) df + (1 - \bar{c}) \int_0^1 \phi_u(f) p(f) df \tag{46}$$

The chemistry calculations and PDF integrations for the burned mixture are calculated in ANSYS FLUENT and the look up tables are created. The laminar flame speeds are measured from experimental data collected. Ansys fluent has determined laminar flame speed curves for $H_2$, $CH_4$, $C_2H_2$, $C_2H_4$, $C_2H_6$ and $C_3H_8$. Mixtures with a limit greater than the rich limit or leaner than the lean flammability limit will not burn and have a flame speed of zero.

## 2.11 Composition PDF Transport

ANSYS FLUENT provides a PDF transport model for computing chemistry effects in turbulent flames. ANSYS FLUENT has two methods for the discretisation of the composition PDF transport model, Lagrangian and Eulerian. Whilst the Lagrangian model is more accurate, it takes significantly longer to converge. The turbulent combustion is governed by the the Navier-Stokes equations, however the direct solutions take too long to compute. ANSYS FLUENT uses a derived transport equation for the probability density function given by:

$$\frac{\partial}{\partial t}\rho P + \frac{\partial}{\partial x_i}(\rho u_i P) + \frac{\partial}{\partial \psi_k}(\rho S_k P) = -\frac{\partial}{\partial x_i}\left[\rho\langle u_i''|\psi\rangle P\right] + \frac{\partial}{\partial \psi_k}\left[\rho\left\langle \frac{1}{\rho}\frac{\partial J_{j,k}}{\partial x_i}\middle|\psi\right\rangle P\right] \tag{47}$$

Where $P$ is the Favre joint PDF of composition, $\rho$ the mean fluid density, $u_i$ Favre mean fluid velocity vector, $S_k$ the reaction rate for species $k$, $\psi$ is the composition space vector, $u_i''$ is the fluid velocity fluctuation vector, $J_{j,k}$ is the molecular diffusion flux vector. vector. Whilst the terms on the left hand side of equation 47 are closed, the terms on the right hand side require modelling. From left to right the terms on the left hand side of the equation are the unsteady rate of change of the PDF, the change of the PDF due to convection and the change due to chemical reactions. On the right hand side the first term is change due to scalar convection by turbulence and the second term is the change due to molecular diffusion. The PDF change due to scalar convection by turbulence is given by:

$$-\frac{\partial}{\partial x_i}\left[\rho\langle u_i''|\psi\rangle P\right] = \frac{\partial}{\partial x_i}\left(\frac{\rho\mu_t}{Sc_t}\frac{\partial P}{\partial x_i}\right) \tag{48}$$

The Lagrangian method can be used to solve the N+1 dimensional PDF transport equation and consists of a convection, diffusion and reaction steps. The convection step is split into two parts, in the first step particles are updated to a new position:

$$x_i^{1/2} = x_i^0 + \frac{1}{2}u_i^0\Delta t \tag{49}$$

Where $x_i$, $u_i$ and $\Delta t$ are the particle position vector, Favre mean fluid velocity vector at the particle position and particle time step respectively. For unsteady flows the particle time step is also the physical time step, in steady-state flows local time steps are calculated per cell:

$$\Delta t = min(\Delta t_{conv}, \Delta t_{diff}, \Delta t_{mix}) \tag{50}$$

The second step, after the diffusion and reaction steps have occurred, is calculated as:

$$x_i^1 = x_i^{1/2} + \Delta t\left(u_i^{1/2} - \frac{1}{2}u_i^0 + \frac{1}{\rho Sc_t}\frac{\partial \mu_t}{\partial x_i} + \xi\sqrt{\frac{2\mu_t}{\rho\Delta t Sc_t}}\right) \tag{51}$$

Where $\rho$ is the mean cell density, $u_i$ is the mean fluid-velocity vector at the particle position, $\mu_t$ is the turbulent viscosity, $Sc_t$ is the turbulent Schmidt number and $\xi$ is the standardised normal random vector.

For the next step, molecular diffusion, ANSYS FLUENT provides three models, the modified curl model, the IEM model and the EMST Model. In the curl model pairs of particles are selected at random, with number of pairs selected being given by:

$$N_{pair} = \frac{1.5C_\phi N\Delta t}{\tau_t} \tag{52}$$

Where $N$, $C_\phi$ and $\tau_t$ are the number of particles, the mixing constant and the turbulent time scale respectively. A particles composition, $\phi$, is moved towards the pairs mean composition by a factor proportional to .

$$\begin{aligned} \phi_i^1 &= (1-)\phi_i^0 + \frac{\phi_i^0 m_i + \phi_j^0 m_j}{m_i + m_j} \\ \phi_j^1 &= (1-)\phi_j^0 + \frac{\phi_i^0 m_i + \phi_j^0 m_j}{m_i + m_j} \end{aligned} \tag{53}$$

Where $mi$ and $m_j$ are masses of particles i and j.

The Interaction by Exchange with the Mean, IEM, model moves the composition of all particles a small distance to the mean composition.:

$$\phi^1 = \phi^0 - (1 - e^{-0.5C_\phi/\tau_t})(\phi^0 - \tilde{\phi}) \tag{54}$$

Where $\phi^0$, $\phi_1$ and $\tilde{\phi}$ are the composition before mixing, the composition after mixing and the Favre mean-composition vector at the particles location.

The Euclidean Minimum Spanning Tree model mixes pairs particles that close to each other in space. The pairing is determined by a Euclidean minimum spanning tree which identifies the minimum length connecting one particle to another.

For the reaction step the reaction source term, $S$ is integrated as:

$$\phi^1 = \phi^0 \int_0^{\Delta t} S dt \tag{55}$$

Where $\phi = (Y_1, Y_2, ..., Y_N, T, p)$ and T is temperature and p is pressure.

Whilst the Langrangian method solves the PDF transport equation by tracking particles through cell, the Eulerian method however, assumes a shape for the PDF and solves the transport equation implicitly. This reduces computation costs. For the Eulerian method the turbulent scalar flux and molecular mixing terms must be modelled. The composition PDF of $N+1$ dimension is represented as $N_e$ delta functions. The form of the PDF is as given by:

$$P(\psi, \overrightarrow{x}, t) = \sum_{n=1}^{N_e} p_n(\overrightarrow{x}, t) \prod_{k=1}^{N_s} \sigma[\psi_k - < \phi_k >_n (\overrightarrow{x}, t) \tag{56}$$

By substituting this equation into equation 47 we obtain the following transport equations for probability and probability weighted conditional mean of composition $k$ respectively:

$$\frac{\partial \rho p_n}{\partial t} + \frac{\partial}{\partial x_i}(\rho u_i p_n) = \nabla(\rho \Gamma \nabla p_n) \tag{57}$$

$$\frac{\partial \rho s_{k,n}}{\partial t} + \frac{\partial}{\partial x_i}_{\rho} u_i s_{k,n} = \nabla(\rho \Gamma \nabla s_{k,n}) + \rho(Mk, n + Sk, n + C_{k,n}) \tag{58}$$

Where $p_n$ is the probability of the nth delta function and $S_k, n$ is the species weighted conditional mean composition of the nth delta function. $\Gamma$ is the turbulent diffusivity and $M_{k,n}$, $S_{k,n}$ and $C_{k,n}$ represent mixing, reaction and correction terms. The reaction term, $S_{k,n}$ is given by:

$$S_{k,n} = \rho_n S(< \phi_k >_n)_k \tag{59}$$

The mixing term is given by:

$$M_{k,n} = \frac{C_\phi}{\tau}(< \phi_k >_n - \psi_k) \tag{60}$$

$C_{k,n}$ is determined from:

$$\sum_{n=1}^{N_e} < \phi_k >_n^{m_k - 1} C_{k,n} = \sum_{n=1}^{N_e} (m_k - 1) < \phi_k >_n^{m_k - 2} p_n c_{k,n} \tag{61}$$

Where $m_k$ are non-negative integer lower moments and $c_k, n$ is given by:

$$c_{k,n} = \Gamma \nabla(< \phi_k >_n) \cdot \nabla(< \phi_k >_n) \tag{62}$$

Mean composition, $k$, and its variance is calculated from:

$$\bar{\phi}_k = \sum_{n=1}^{N_e} s_{k,n} \tag{63}$$

$$\bar{\phi}_k'^2 = (\sum_{n=1}^{N_e} s_{k,n} < \phi_k >_n) - \bar{\phi}_k^2 \tag{64}$$

## 2.12 Engine Ignition

The ignition model of interest to this report is the spark ignition model. The transport equation for the mean reaction progress term, $c$ is given by:

$$\frac{\rho c}{\partial t} + \nabla \cdot (\rho \overrightarrow{v} c) = \nabla \cdot (D_t \nabla_c) + \rho_u U_t |\nabla c| \tag{65}$$

$D_t$, $\rho_u$, $U_t$ are the diffusivity, density of the mixture and turbulent flame speed. Due to the small spark size relative to the mesh size this equation is modified to become:

$$\frac{\rho c}{\partial t} + \nabla \cdot (\rho \overrightarrow{v} c) = \nabla((\kappa + D_{tt}) \nabla c) + \rho_u U_t |\nabla c| \tag{66}$$

where $\kappa$ is the laminar thermal diffusivity and the $D_{tt}$ is the effective diffusivity.

## 2.13 NOx Formation

The formation of $NO$, $NO_2$ and $N_2O$ can be modelled in ANSYS FLUENT in order to aid in the design of $NOx$ control measures. To predict $NOx$ ANSYS FLUENT solves a transport equation for $NO$. $NOx$ is post-processed from the combustion simulation, thus requiring the combustion simulation to be accurate in order to predict $NOx$. There are four main chemical processes that result in $NOx$ production, thermal $NOx$, Prompt $NOx$, Fuel $NOx$ and intermediate $N_2O$. Given this report uses hydrogen as a fuel the Prompt $NOx$ and Fuel $NOx$ models will not be included in this section as the fuel $H_2$ does not contribute to these models.

Formation of thermal $NOx$ is controlled by the Zeldovich mechanism. The reactions which cause thermal $NOx$ to occur are:

$$\begin{aligned} O + N_2 &\leftrightarrow N + NO \\ N + 0_2 &\leftrightarrow O + NO \\ N + OH &\leftrightarrow H + NO \end{aligned} \tag{67}$$

The rate constants $k_{f,1}$, $k_{f,2}$, $k_{f,3}$, $k_{r,1}$, $k_{r,2}$, $k_{r,3}$ for the reactions have been selected based on from the work of Hanson and Salimian ,1984. Values with subscript $f$ denote forward reactions, subscript $k$ denote reverse reactions.

$$\begin{aligned} k_{f,1} &= 1.8x10^8 e^{-38370/T} & k_{r,1} &= 3.8x10^7 e^{-425/T)} \\ k_{f,2} &= 1.8x10^4 T e^{-4680/T} & k_{r,2} &= 3.81x10^3 T e^{-20820/T} \\ k_{f,3} &= 7.1x10^7 e^{-450/T} & k_{r,3} &= 1.7x10^8 e^{-24560/T} \end{aligned}$$

Thus the rate of formation of $NO$ is given by:

$$\frac{d[NO]}{dt} = k_{f,1}[O][N_2] + k_{f,2}[N][O_2] + k_{f,3}[N][OH] - k_{r,1}[NO][N] - k_{r,2}[NO][O] = k_{r,3}[NO][H] \tag{68}$$

With sufficient oxygen the rate of consumption of free nitrogen becomes equal to rate of its formation, allowing us to assume a steady state in all but the most rich combustions. Thus the $NO$ rate becomes:

$$\frac{d[NO]}{dt} 2k_{f,1}[O][N_2] \frac{\left(1 - \frac{k_{r,1}k_{r,2}[NO]^2}{k_{f,1}[N_2]k_{f,2}[0_2]}\right)}{\left(1 + \frac{k_{r,1}[NO]}{k_{f,2}[0_2]+k_{f,3}[OH]}\right)} \tag{69}$$

In order to calculate equation **??** the concentration of $O$ and $OH$ are necessary. To determine the $O$ concentration ANSYS FLUENT uses one of three approaches, the equilibrium method, the partial equilibrium method and the predicted $O$ approach. The equilibrium method obtains $O$ from the equation:

$$[O] = k_P[O]^{1/2} = 3.97x10^5 T^{1/2}[O_2]^{1/2} e{-}31090/T \tag{70}$$

The partial equilbirium method finds $O$ as:

$$[O] = 36.64T^{1/2}[O_2]^{1/2} e^{-27123/T} \tag{71}$$

Finally, when using an advance chemistry model, such as the flamelet submodel the value of $O$ can predicted using the local species mass fraction. The $OH$ concentration is also predicted using three models, the first approach involves assuming it is negligible and excluding it from the calculation and is valid for lean combustion. The partial equilibrium method calculates the concentration of $OH$ using this equation:

$$[OH] = 2.129x10^2 T^{-0.57} e^{-4595/T}[O]^{1/2}[H2O]^{1/2} \tag{72}$$

Finally the predicted $OH$ model, similar to the predicted $O$ model uses the local species mass fraction.

$NOx$ formation from intermediate $N_2O$ is given by the equation:

$$\frac{d[NO]}{dt} = 2\left(k_{f,2}[N_2O][O] - k_{r,2}[NO]^2\right) \tag{73}$$

As in the $NO$ model, the concentration of $O$ and $N_2O$ are required. $N_2O$ is assumed to be steady at quasi steady state which leads to the equation:

$$[N_2O] = \frac{k_{f,1}[N_2][O][M] + K_{r,2}[NO]^2}{k_{r,1}[M] + K_{f,2}[O]} \tag{74}$$

Where:

$$\begin{aligned} k_{f,1} &= 4.44x10^{32} T^{-8.358} e^{-28234/T} & k_{r,1} &= 4.00x10^8 e^{-28234/T} \\ k_{f,2} &= 2.90x10^7 T^{11651/T} & k_{r,2} &= 1.45x10^{-29} T^{9.259} e^{11651/T} \end{aligned}$$

# 3 Methodology

## 3.1 CFD

### 3.1.1 Overview

The process of creating a CFD simulation of the Wankel engine combusting hydrogen can be divided into three key areas, preparing the geometry, preparing the mesh and preparing the simulation. The geometry was prepared using CAD files for the AIE 80S engine from which the fluid geometry was extracted. The mesh was created in Ansys meshing due to it being integrated into the Ansys Workbench software. The simulation was prepared and run in Ansys Fluent

### 3.1.2 Geometry

The geometry used is that of the Advanced Innovative Engineering (AIE) 80S, an 80cc, single rotor Wankel rotary engine with a compression ratio of 9.6:1. AIE has provided computer aided design (CAD) models for the rotor with simplified apex seals and the casing with inlet and exhaust ports and spark plug positions. Using SOLIDWORKS these CAD models were used to create the geometry of the fluid in the engine, Figure 1 shows the geometry in SOLIDWORKS. Whilst the majority of the fluid geometry is identical to that of the 80S, the apex seals have been simplified to cylinders with a small gap of 0.2mm left between the tip of the apex seals and the casing. The apex seals have been simplified to avoid complex geometry. The gap is necessary as the dynamic mesh in Ansys fluent requires that one layer of cells remains between surfaces to maintain topology.

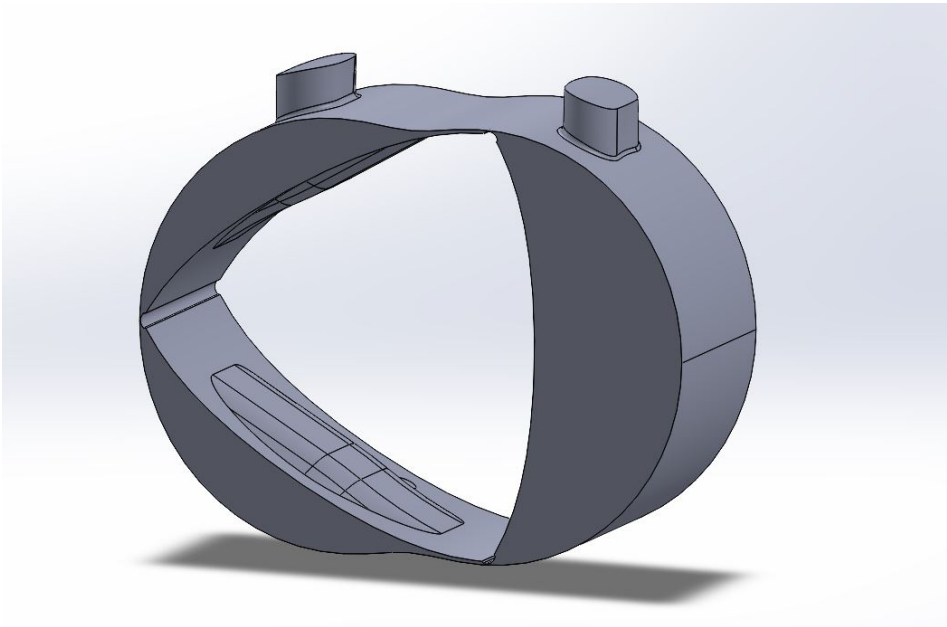

Figure 1: Geometry of the fluid in the AIE 80S rotary engine.

The geometry was next imported into Ansys Spaceclaim in order to be repaired and prepared for meshing. During this step the surface topography was not changed. However, due to the transfer from solidworks to Spaceclaim additional features may have been generated which could be removed for an improved model. The primary concern for this study was that the surfaces where the spark plugs would enter were missing, Spaceclaim's missing surfaces tool was used to fill in these missing surfaces. Given that the engine has one axis of symmetry the fluid geometry was also bisected length ways in order to reduce computation times.

### 3.1.3 Meshing

The geometry was next imported into Ansys Meshing. Due to limitations in the dynamic meshing of Ansys Fluent the tetrahedrons method had to be selected, this results in tetrahedral shaped elements. The small displacement of the 80S engine, coupled with its single axis of symmetry means that an accurate mesh can be generated without significantly compromising computation times. The cells of primary concern for accuracy are situated at the tip of the apex seals, this is due to the small gaps resulting in highly skewed cells which will affect the accuracy of the simulations. Additionally, on the face of the rotor in the exhaust stroke at start time there is issues with the surface topography, resulting in highly skewed cells if it is not accounted for with an increased cell count on this surface.

A number of different meshing techniques and qualities were assessed for the use in this report. The body of influence method required the creating of a body of influence around the area we are of most interest. This was done using the equations of a rotary engine described by Yamamoto (1981) and introducing it to Spaceclaim, and

from there into the mesher. By introducing a sizing method to mesh and selecting body of influence (BOI) from the dropdown the BOI can be designated. The BOI sizing allows you to set the size of all cells within the BOI.

Face sizing is another method that can be used to control the size of the cells. The faces that are to be different sizes are selected and from there the cell size can be set. As ANSYS FLUENT cannot remesh face cells on static walls it is important to maintain a high density mesh on the casing faces, opposite the rotor and at the rotor tips, where the walls of the rotor casing face will be in close proximity. This increases the quality of the cells in this area.

Another limitation on the meshing is that in order to prevent flame propagation between combustion chamber no more than two layers of cells can generate at the rotor tips. This is due to ANSYS FLUENT not calculating wall quenching behaviour and instead providing a factor that lowers the flame speed on wall adjacent cells. Furthermore, this means for realism wall adjacent cells should not be too large or too small relative to the quenching distance of the fuel used. This is to prevent unrealistic quenching of the combustion calculation. For this study the wall cells must be around 0.3mm in height to prevent unrealistic quenching. For a regular tetrahedron this is around 0.73mm of cell length.

## 3.2 Rotor Movement

The rotor movement is controlled by a User Defined Function, written in C. The rotors movement is described by an eccentric rotation about the crank shaft. For the AIE 80S engine the rotors offset is 7.7mm. At 9000RPM at the crankshaft the UDF is given by:

```
# include "udf.h"
#define r -0.0077 /*Eccentricity*/

/* for grid motion */
DEFINE_CG_MOTION(rotor, dt, vel, omega,time, dtime)
{
real beta;

NV_S(vel, =, 0.0);
NV_S(omega, =, 0.0);

omega[2] = 314.159; /*angular velocity in rad/sec*/
beta = 942.477; /*angular velocity of rotor in rad/sec*/

vel[0] = -beta*r*sin(beta*time);
vel[1] = beta*r*cos(beta*time);
vel[2]= 0;

}
```

### 3.2.1 Simulation Setup

In order to run the simulation, a transient, pressure-based formulation was selected. The energy equation, $k - \epsilon$ turbulence model and partially premixed combustion models were selected. Spark ignition and NOx models were also used for the combustion. The pressure-velocity coupling method was the PISO scheme with no coupling. The gradient was Least Squared cell based and all other formulas were second order. The operating pressure for the interior has been set to zero and the inlet pressure was been set to 101325 Pa, at a temperature of 300K and with the intensity and hydraulic diameter turbulence specification method selected. The hydraulic diameter was set to 13mm and the intensity to 1%. For the $k - \epsilon$ model the realizable model has been used, with standard wall functions. For the partially premixed combustion the steady diffusion flamelet state relation has been used. The Chemkin mechanism file for the combustion has been obtained from Nozari and Karabeyoglu (2015). Hybrid initialization has been used to initialize the simulation however as the chamber at 30 degrees before top dead centre's pressure is unknown and no turbulence effects can be introduced prior to calculation it has been set to 101325 Pa, and planned for no combustion to occur. The spark timing has been to set to align with five degrees before top dead centre for the chamber which begins 120 degrees before top dead centre. The NOx models used were thermal NOx and the N2O intermediary, both set to partial equilibrium. Given the wall quenching is not modelled in ANSYS FLUENT a constant which modifies flame speed in wall adjacent cells is available, the value of this has been set to 0 to prevent flame propagation between chambers. For the dynamic mesh a max length of 0.002m and minimum length of 0.0002m has been selected to maintain a high quality mesh. The cell skewness and face skewness have been set 0.7, this results in slightly longer meshing time but results in a higher quality mesh. A number of different time steps have been experimented with to achieve a balance between quality and simulation time and a time step of 5.5556e-6 has been selected. This is 0.1 degrees per time step of rotor rotation. Meaning a full rotation requires 3600 time steps. For this simulation only 240 degrees of rotation are necessary to find the MEP as each chamber is performing a step of the cycle, offset by 120

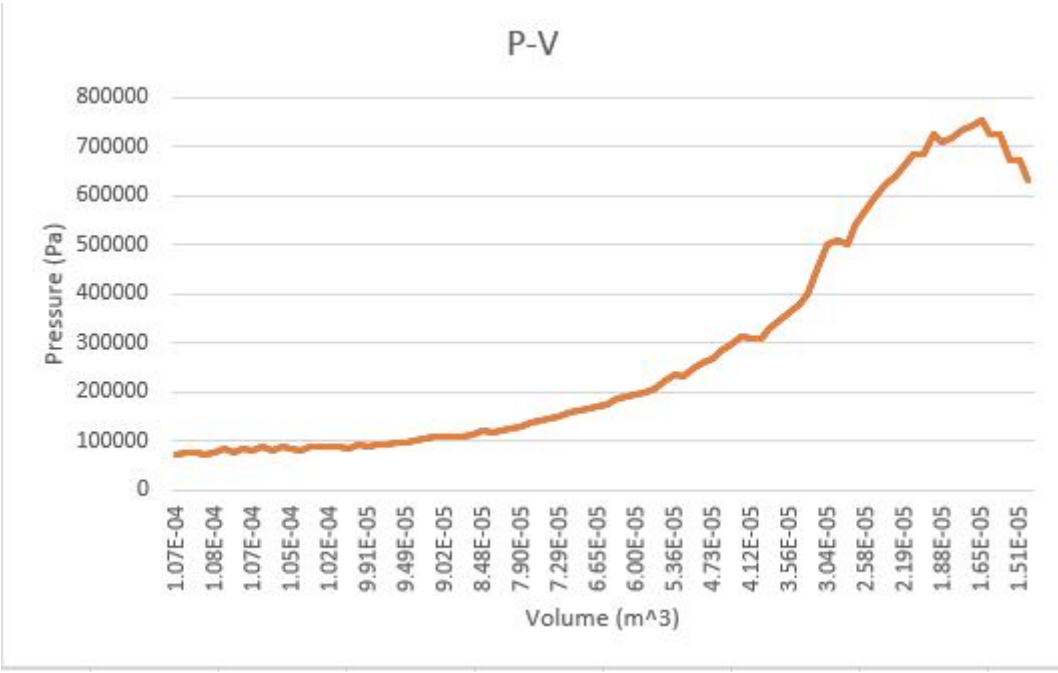


Figure 2: Pressure-volume diagram of the compression stroke.

degrees from each other.

### 3.3 Data Analysis

Indicated Mean Effective Pressure is a useful tool as it allows comparison of different engine and fuel setups with accounting for displacement. The MEP is thought to be the average pressure applied to the piston across its cycles. In the case of the rotary engine, the piston is the rotor. By measuring the average pressure on the surface of the rotor and calculating the volume of the cylinder we can plot the change in pressure against volume. We can find the work done by the gas on the rotor by integrating under the curve.

## 4 Results

Unfortunately, due to time constraints and hardware limitations the pressure data was only collected for the compression stroke of the cycle, as such this section will only serve as a proof of concept for more in depth studies.

Figure 2 shows the pressure acting on the rotor and volume of the chamber from the start to the end of the compression stroke. By integrating under this curve we can obtain the work done on the gas by the rotor, which comes to 2.1081kW. If the simulation were continued through the other steps of the otto cycle a value for the indicated work per cycle could be obtained. Dividing the indicated work per cycle by the displacement of the engine would provide the mean effective pressure of the system, ignoring frictional effects.

## 5 Discussion

Validation of the pressure data generated from ANSYS FLUENT was originally intended to be done via experiment using transistors to collect limited pressure data from the spark plugs. Unfortunately this was unable to be performed as the physical engine was not ready in time. Instead the pressure data can be compared to the known compression ratio of the engine, 8.6. Whilst this does not provide in depth information which would be required for more in depth study it is sufficient to demonstrate the method used. The graph shown in Figure 2 shows an increase in pressure with a decrease in volume until to the end of the cycle. This is due to apex seal leakage as due to limitations with ANSYS FLUENT, the rotor wall and casing wall cannot touch. Furthermore the decrease in pressure as peak compression is achieved is also in part due to sinusoidal compression stroke resulting in the leakage over taking the rate of compression. The stated compression ratio of the AIE 80S engine is 9.6:1 whereas the ratio of maximum pressure to initial pressure is 7.22:1, this is mostly likely due to the overemphasized apex seal leakage. Furthermore the model used to collect this was not particularly accurate, meaning the mesh quality was lower than was recommended in the methodology section, at 2mm length, and the time step could be reduced from the $5.556x10^{-}6$ to improve accuracy further. This likely overemphasized the leakage that occurred at the seals. Whilst the method can be used to obtain pressure data inside a Wankel rotary engine it will not replace actual experimental data and should only be used in addition to real pressure data to lower the cost of investigations into the engine.

## 5.1 Viability of the Engine

The suitability of a hydrogen powered Wankel rotary engine for use in a motorcycle is dependent on the following factors: Emissions, power and range. The emissions will be affected by the temperature in the engine and amount of lubricant necessary to run the maintain the engine whilst running. The power is affected by the combustion characteristics, temperature and thermal efficiency of the engine. Range of the engine is affected by the fuel efficiency of the engine, mass of the motorcycle and volume available for storage.

### 5.1.1 Emissions

Whilst hydrogen combustion only creates water, the high temperature environment allows for the formation of $NO_x$. In hydrogen combustion thermal and and $N_2O$ intermediate $NO_x$ formation are the primary concerns. Given the effect $NO_x$ has on global warming is 310 times greater than that of carbon dioxide and causes significant health issues (Hosseini et al,. 2012) it is paramount this is minimised. Given the direct relationship between $NO_x$ and temperature reduction of temperature is necessary. This can be achieved through lean combustion, slowing combustion speed and is also achieved through the geometry of the rotary engine design. The rotation of the chamber in the direction of combustion serves to effectively slow down the rate of combustion as it must pursue the rotor. This serves to increase total distance the flamefront must travel, reducing the overall temperature. $NO_x$ emissions are not the only concern in Wankel rotary engines as the engine must have lubricant in the chamber to avoid wear. The amount of lubricant necessary is however, significantly reduced through the combustion of hydrogen as hydrogen combustion does not generate soot or carbon deposits on the surface of the engine. Additionally, the use of ceramic apex seals can further reduce the need for lubricant by minimising friction between the apex seals and the casing face. The few emissions generated from the combustion process can then be run through a catalytic converter to finally minimise the overall emissions. Whilst, from the current body of research, it seems impossible to reduce the emissions from hydrogen combustion to zero the author believes they can be sufficiently lowered to an acceptable level.

### 5.1.2 Power

The power to weight ratio of a Wankel rotary engine has always been higher than that of a conventional reciprocating engine. However, due to significant amounts of unburned fuel in the exhaust and low thermal efficiency with gasoline as a fuel it has not been used. The combustion characteristics of hydrogen serve to offset the issue of unburned fuel as it able to combust before reaching the exhaust. The necessity of running hydrogen lean to reduce overall emissions however, serves to lower the power of the engine. Wakayama, et al (2006) found that the RENESIS duel fuel rotary engine had a 48% reduction in peak power, from 154kW on gasoline to 80kW using hydrogen however that was whilst running the hydrogen fuel with an excess air ratio of 1.6. They found that compared to the gasoline hydrogen had a 23% improved fuel economy. When comparing the power trade off between a reciprocating engine and the hydrogen Wankel engine the reduction in power will become less significant. Additionally, whilst engine power can be a draw for some motorcycle audiences, especially amonst those that ride as a hobby. One method to offset the power loss would be to use a larger engine, effectively offsetting the power loss relative to reciprocating engines by taking advantage of the small volume and weight of the rotary engine. Those who use the motorcycle more regularly tend to use lower power, more fuel efficient motorcycles and thus would be more like to trade off power in order to be more eco-friendly. For this to be true any hydrogen fuelled motorcycle would need to be low cost and the infrastructure to support it would need to built.

### 5.1.3 Range

The range of the hydrogen fuelled motorcycle is likely to be the primary area of concern, especially prior to the mass adoption of hydrogen fuel pumps in countries. A conventional motorcycle fuel tank holds about 10 litres of fuel, which at 700 bar of pressure (NPROXX presents new 700 bar hydrogen tank to the automotive industry, 2019), would hold 420g of hydrogen. This is $5.95x10^7$J of energy. The harley davidson livewire, an electric motorcycle has a batter with a capacity of 15.5kwh, or $5.56x10^7$J of energy (Harley-Davidson, n.d.). The motorcycle however, weighs 254kg, of which most of the weight comes from the battery, significantly reducing the range of vehicle. It is thus clear that hydrogen storage is significantly more energy dense than that of a battery. Unfortunately the combustion process of a rotary engine is significantly less efficient than that of the electric motorcycle, which is like to offset the benefits of having a low mass fuel. Electric power trains can be up to 70% efficient whilst the best combustion engines remain around 40% efficient, fuel cells are around 40 to 60% efficient depending on the type used. The lower fuel efficiency of the Wankel rotary power train is offset by its weight. Fuel cell and electric power train systems are often heavy, requiring bulky packs of batteries or fuel cells and complicated temperature management systems to reduce wear.

# 6 Conclusions

The Wankel rotary engine is likely to be a strong candidate for an eco-friendly power-train, be it used in series-hybrid or directly through the transmission. Its capability for low emission combustion of hydrogen when using lean combustion has begun to make it of more interest to industry for use in automotive purposes. Whilst there does not currently

exist a commercially available hydrogen rotary engine motorcycle, the technologies which will facilitate its existence are being investigated in depth for use in other parts of the automotive industry, such as fuel cell motorcycles. From the body of research that currently exists it is impossible for Wankel rotary engines to achieve zero emissions, due to trace amounts of NOx production and necessity to burn lubricant. However, relative to a hydro-carbon fuel, a hydrogen fuelled engine will require less lubricant as carbon deposits are not generated on the surface. A significant concern to use of hydrogen in motorcycles in the safety of the system, reducing the chance of accidents resulting from a hydrogen gas leak means hydrogen sensors are necessary to be installed near the valves and impact testing must be performed on any motorcycle prior to production. However, many in the automotive industry have performed such tests for fuel cell cars and found little issue with the system. Whilst the Wankel rotary engine is not the perfect solution to a zero-emission future the author believes it is one worth exploring in greater detail. Ultimately the use of hydrogen in a Wankel rotary engine comes at the cost of power and range in exchange for a simple, reliable, knock resistant engine with significantly lower emissions than piston driven alternatives. With the simple design meaning it is likely to be cheap to manufacture, especially given the primary material used is steel, making it a more affordable option compared to fuel cell and battery vehicles which use rare metals and complicated manufacturing techniques.

# 7 Further Work

In order to fully explore the possibility for a Wankel rotary engine to be used in a motorcycle, a number of experimental tests need to be performed such as running an engine at different loads to determine how emissions may change with RPM and allow for different methods of counteraction to be devised. The effects of direct injection, injection position and direction on combustion. Investigation into the how the shape of the rotor recess can affect turbulence and combustion. The construction and design of a motorcycle that uses Wankel Rotary Engine that uses hydrogen as a fuel is feasible however there is a large number of issues which must be investigated before it can be used a truly eco-friendly alternative. The methods outlined in this report can be used to facilitate many of these techniques, in particular injection and turbulence effects by a team with the hardware necessary to do so. The author highly recommends any in depth CFD work in the future is performed with access to a server cluster to significantly decrease simulation times as for this simulation which uses a r

# References


[1] Wakayama, N., Morimoto, K., Kashiwagi, A. and Saito, T. (2006). Development of Hydrogen Rotary Engine Vehicle.

[2] Cichanowicz, J.E. and Sawyer, R.F. (1976). Rotary Engine Combustion With Hydrogen Addition. SAE Technical Paper Series.

[3] Salanki, P.A. and Wallace, J.S. (1996). Evaluation of the Hydrogen-Fueled Rotary Engine for Hybrid Vehicle Applications. SAE Technical Paper Series.

[4] Advanced Innovative Engineering (UK) Ltd. (2015). 80S – 15 BHP. [online] Available at: https://www.aieuk.com/80s-15bhp-wankel-rotary-engine/ [Accessed 14 Mar. 2022].

[5] Transitioning to zero emission cars and vans: 2035 delivery plan Contents. (n.d.). [online] Available at: https://assets.publishing.service.gov.uk/government/uploads/system/uploads/attachment data/file/1005301/transitioning to-zero-emission-cars-vans-2035-delivery-plan.pdf.

[6] www.crightonmotorcycles.com. (n.d.). The Machine. [online] Available at: https://www.crightonmotorcycles.com/the-machine [Accessed 14 Mar. 2022].

[7] McKie, R. (2021). Child labour, toxic leaks: the price we could pay for a greener future. [online] The Guardian. Available at: https://www.theguardian.com/environment/2021/jan/03/child-labour-toxic-leaks-the-price-we-could-pay-for-a-greener-future.

[8] Lipatnikov, A.N. and Chomiak, J. (2002). Turbulent flame speed and thickness: phenomenology, evaluation, and application in multi-dimensional simulations. Progress in Energy and Combustion Science, [online] 28(1), pp.1–74. doi:10.1016/S0360-1285(01)00007-7.

[9] Hanson, R. and Salimian, S. (1984). Survey of Rate Constants in H/N/O Systems. Combustion Chemistry, p.361.

[10] Yamamoto, K. (1981). Rotary engine. Tokio: Sankaido Co.

[11] Sierens, R., Baert, R., Winterbone, D.E. and Baruah, P.C. (1983). A Comprehensive Study of Wankel Engine Performance. SAE Technical Paper Series.

[12] Farzadi, A. (2015). FLOW ANALYSIS IN WANKEL TYPE ROTARY ENGINE.

[13] Salvi, B.L. and Subramanian, K.A. (2016). Experimental investigation on effects of compression ratio and exhaust gas recirculation on backfire, performance and emission characteristics in a hydrogen fuelled spark ignition engine. International Journal of Hydrogen Energy, 41(13), pp.5842–5855.

[14] Di Ilio, G., Bella, G. and Jannelli, E. (2020). Performance Evaluation of Extended-Range Electric Vehicles Equipped with Hydrogen-Fueled Rotary Engine. SAE Technical Paper Series.

[15] Cracknell, R., Alcock, J., Rowson, J., Shirvill, C. and Ung ut, A. (2002). Safety Considerations in Retailing Hydrogen. SAE Transactions, [online] 111, pp.922–926. Available at: https://www.jstor.org/stable/44734577.

[16] MUROKI, T. and FUJIMOTO, Y. (1987). Unburned hydrocarbon emissions of Wankel type rotary piston engine. (1st report The source of unburned hydrocarbon). TRANSACTIONS OF THE JAPAN SOCIETY OF MECHANICAL ENGINEERS Series B, 53(485), pp.306–310.

[17] Li, Z., Shih, T.I-P., Schock, H.J. and Willis, E.A. (1991). A Numerical Study on the Effects of Apex Seal Leakage on Wankel Engine Flow Fields. SAE Technical Paper Series.

[18] Ohkubo, M., Tashima, S., Shimizu, R., Fuse, S. and Ebino, H. (2004). Developed Technologies of the New Rotary Engine (RENESIS). SAE Technical Paper Series.

[19] www.crightonmotorcycles.com. (n.d.). The Machine. [online] Available at: https://www.crightonmotorcycles.com/the-machine [Accessed 14 Mar. 2022].

[20] Heywood, J.B. (2018). Internal combustion engine fundamentals. New York: Mcgraw-Hill Education.

[21] Vorraro, G., Turner, M. and Turner, J.W.G. (2019). Testing of a Modern Wankel Rotary Engine - Part I: Experimental Plan, Development of the Software Tools and Measurement Systems. SAE Technical Paper Series.

[22] NPROXX presents new 700 bar hydrogen tank to the automotive industry (2019) FuelCellsWorks. Available at: https://fuelcellsworks.com/news/nproxx-presents-new-700-bar-hydrogen-tank-to-the-automotive-industry/ (Accessed: July 26, 2022).

[23] Meng, H., Ji, C., Yang, J., Chang, K., Xin, G. and Wang, S. (2022). A knock study of hydrogen-fueled Wankel rotary engine. Fuel, 321, p.124121. doi:10.1016/j.fuel.2022.124121.

[24] Hosseini, S.E., Wahid, M.A. and Abuelnuor, A.A.A., 2012. High temperature air combustion: sustainable technology to low NOx formation. International Review of Mechanical Engineering, 6(5), pp.947-953.

[25] Harley-Davidson. (n.d.). LiveWire Motorcycle — Harley-Davidson United Kingdom. [online] Available at: https://www.harley-davidson.com/gb/en/motorcycles/2021/livewire.html.

[26] EDF. (n.d.). Feel the burn: why EVs are more efficient than any fuel-burning car. [online] Available at: https://www.edfenergy.com/for-home/energywise/why-EVs-are-efficient.